Modelling PLN R14del cardiomyopathy using hiPSC-derived cardiac spheroids and organoids

Adriana Silva Passadouro
adriana.passadouro@tecnico.ulisboa.pt

Instituto Superior Técnico, Lisboa, Portugal

3^{rd} November 2021

Abstract

Cardiomyopathies are a group of structural and functional disorders of the heart muscle that often lead to heart failure, caused by combined genetic and acquired triggers. Phospholamban (PLN) is a cardiac protein involved in Ca^{2+} homeostasis in cardiomyocytes (CMs), being a crucial regulator of cardiac contractility. Deletion of arginine 14 in the PLN gene (R14del) cardiomyopathy is a severe, not yet fully understood disease. R14del is associated with the dilated cardiomyopathy (DCM) phenotype, including ventricular arrhythmias, cardiac fibrosis and sudden cardiac death, with no effective treatment available. Thus, the current *in vitro* systems available fail to translate, not providing a proper insight into the complex dynamics of the human heart. Alternatively, three dimensional (3D) models can recapitulate the native tissue's microenvironment and its pathophysiological conditions, possibly comprising cells derived from human induced pluripotent stem cells (hiPSCs), obtained from patients with specific known genotypes. Specifically, using R14del patient-specific hiPSC-derived CMs can help bridging the disease modelling gap and elucidate on the link between impaired contractility, Ca^{2+} mishandling and the amount of fibrosis in the hearts of PLN R14del patients.

In this project, a new methodology for the generation of cardiac spheroids was developed and a technique for human cardiac organoids (hCOs) generation was adapted and optimised using mutation carrier and healthy cell lines. The systems established permitted the study of 3D cellular architecture, detection of cardiac fibrotic remodelling in PLN R14del, beating rate measurements and Ca^{2+} transients analysis, where a clear contrast was identified between PLN R14del and CTRL.

Keywords: cardiac organoids; cardiac spheroids; cardiomyocytes; PLN R14del; cardiomyopathy.

1. Introduction

Cardiovascular diseases (CVDs), including cardiomyopathies, are the number one cause of death globally, according to the World Health Organization [1]. Thus, they have taken centre stage in many biomedical research projects. Genetic predisposition, such as mutations in Phospholamban (PLN), have a relevant causal link in the development of cardiomyopathies. These pathologies are disorders of the cardiac muscle that cause mechanical and/or electrical dysfunction. Since cardiomyocytes (CMs) are the key component for cardiac contraction which is regulated by Ca^{2+} homeostasis in each CM, it is natural that pathologies linked to a disruption in the beat-to-beat controlled Ca^{2+} handling process amount to a third of all deaths in the developed world [2]. Cardiac development and pathology are regulated by Ca^{2+} signalling pathways acting on gene expression and CM growth, which are also crucial factors for Ca^{2+} homeostasis in the heart. Notably, altered Ca^{2+} underlies a number of pathological events such as inappropriate cardiac growth, rhythmic disturbances and heart failure [2]. Specifically, CM dysfunction and consequent arrhythmias can arise from an increase in cytosolic Ca^{2+} concentration or prolonged intervals of increased Ca^{2+} [3].

The pump function of the heart is mediated by the synchronous contraction of the CMs where intracellular Ca^{2+} handling is a tightly-controlled process to ensure optimal electrical and mechanical CM function. Excitation-contraction coupling (ECC) is the process in which the action potential generated by pacemaker cells is transducted into the CMs' contractile response. Briefly, CM depolarization activates Ca^{2+} entry in the cell via depolarization-activated L-type Ca^{2+} channels (LTCC). Subsequently, Ca^{2+}-induced Ca^{2+} release (CICR) occurs where Ca^{2+} binds to and opens ryanodine receptor type 2 (RYR2), inducing the release of a much larger quantity of Ca^{2+} from the sarcoplasmic reticulum (SR). The increase in cytosolic Ca^{2+} concentration potentiates Ca^{2+} binding to troponin C allowing the thin (actin) and thick (myosin) filaments to interact and develop force, allowing for CM contraction. During diastole (heart's relaxation), Ca^{2+} dissociates from troponin C and its removal from the cytosol occurs due to Sarcoplasmic reticulum Ca^{2+}-ATPase's (SERCA2a) function to reuptake Ca^{2+} back in the SR [2, 4, 5].

PLN is a 52-amino acid protein located in the SR membrane that regulates the SERCA2a pump, reversibly inhibiting its Ca^{2+} affinity [6]. Evidently, mutations in the PLN gene are highly linked to the disruption of the SERCA-induced balance of Ca^{2+} handling. The deletion of arginine 14 codon (R14del) in the PLN gene has an irreversible super-inhibitory effect of SERCA2a activity, resulting in blockage of Ca^{2+} reuptake [7]. PLN R14del, being linked to an impaired Ca^{2+} reuptake and contractility, results in malignant arrhythmias and sudden cardiac death [8, 6]. Interestingly, the R14del mutation appeared to be the most prevalent cardiomyopathy-related mutation in the Netherlands, being present in 15% of patients with dilated cardiomyopathy (DCM) [8]. Arising from a variety of genetic and acquired triggers, the clinical course of patients with DCM is remarkably heterogeneous given distinct pathophysiological features [9]. When compared to other mutation carriers, patients with a PLN mutation have a higher frequency of left ventricle structural and functional abnormalities [8]. Moreover, PLN R14del hearts were compared with hearts with desmosomal, lamin A/C, sarcomeric and desmin mutations and presented the highest amount of myocardial fibrosis (found in a distinct pattern in the posterolateral left ventricle wall) [10]. Ultimately, it has been determined that PLN R14del mutation carriers have higher incidence of malignant ventricular arrhythmias with left ventricular ejection fraction $<$45%, premature sudden cardiac death and end-stage heart failure when compared to DCM patients that do not carry this pathogenic variant [6, 7].

Given the highly variable phenotype of patients with PLN R14del cardiomyopathy, ranging from asymptomatic to cardiomyopathic, the prognosis is significantly poor. Therefore, it is understandable that the assessment of the molecular mechanisms underlying the pathogenesis of the disease becomes an even more difficult task [8]. The previously developed models for this disease have highlighted a few pathological features. Some of this data has even been correlated to the human disease phenotype. However, further elucidation is still needed to connect the phenotype to disease development and severity. Additionally, to date, the link between impaired contractility, Ca^{2+} mishandling and the profound amount of fibrosis found in the hearts of PLN R14del patients remains unknown along with the link between the mutation and the severity of the cardiomyopathy and arrhythmias generated. Nevertheless, in the

past decade, research using animal and standard cellular models has potentiated further understanding into the genetics and physiology of the heart. Complemented by work with cellular models using human pluripotent stem cells (hPSCs), including human embryonic stem cells (hESCs) and hiPSCs, the field is progressing with providing proper insight into the complex dynamics of the human heart as a whole [11, 12, 13, 14, 15].

Specifically, hiPSCs can be an unlimited supply of cells obtained from patients with known genetic diseases. Hence, they can better represent their pathophysiological phenotypes, constituting a clinically-relevant platform for cardio-active drugs screening [16]. Deriving CMs from hiPSCs can be efficiently done through defined small molecule differentiation protocols using chemically defined serum free media, which were reported to have reduced lot-to-lot variability of CMs [17, 18]. Upon cardiac differentiation, the model developed needs to be evaluated for its fundamental characteristics. Taking into consideration either cell-cell and cell-extracellular matrix (ECM) dynamics in the human heart or tissue dynamics between the different cardiac cell layers, there is a high demand for the development of new experimental models that allow for a long-term evaluation of cardiac function in a controlled laboratory setting. Animal models are the most physiological model but there is an imprecise control of complex integrated processes *in vivo* which can mask key underlying mechanisms and present contradictory outcomes. 2D cell cultures on engineered substrates are undoubtedly easier to control than animal models but strikingly non-physiological and present a limited predictability [19]. Instead, 3D systems such as spheroids can provide a microenvironment mimicking the native tissue dynamics and their pathophysiological conditions. This investigation can rarely be performed directly in the organ due to ethical issues and source scarcity. As a result, 3D structures formed by stem cells and consisting of organ-specific cell types have also been developed, called organoids.

Organoids are defined as 3D structures, mimicking tissue and respective organ dynamics and structure. They are composed of organ progenitors or different stem cell types typically present in the organ it intends to resemble with the ability to self-organize through cell sorting and spatially restricted lineage commitment, reflecting organogenesis *in vitro* [20]. These structures are expected to present both functional similarities and homologous gene expression profiles compared to their *in vivo* tissue counterpart [21]. Importantly, as spheroids and organoids can be derived from hiPSCs either from healthy donors or patients, using Clustered Regularly Interspaced Short Palindromic Repeats (CRISPR)-Cas9 technology, they can be applied for not only disease modelling but also patient-specific drug screening. Therefore, they represent highly relevant technologies to be applied for personalized medicine [22].

Hence, 3D models are incredibly pertinent for PLN R14del cardiomyopathy, for which there are no specific therapeutic treatment options available. Current guidelines for heart failure and ventricular arrhythmias are followed, where, unfortunately, the therapeutic option for this cardiomyopathy is heart transplantation. This is not a lifetime solution as the average lifespan of a heart transplant is 9.16 years [23]. In attempts to advance the field, studies in human mutation carriers are laborious, expensive and strikingly long, explaining the urgent need for efficient, physiological, robust and reproducible disease models. This way, the field is progressing towards recapitulating complex cardiac disorders and to engineer 3D models of the heart *in vitro*.

Therefore, the following thesis aims to elucidate the molecular mechanisms related to the PLN R14del phenotype in a 3D context establishing cell-based systems for 3D culturing of proliferative CMs derived from hiPSCs. Using this culturing platform, it is expected that the 3D model contributes to a better understanding of the disease phenotype and can constitute a robust middle-high throughput screening platform for novel therapeutic strategies to cure the PLN R14del disease.

2. Materials and Methods

2.1. Cardiac spheroids and organoids generation

Two previously established hiPSC lines (SCVI-273, Sendai virus reprogrammed, peripheral blood mononuclear cells (PBMCs), female [24] and PLN R14del patients [25] were grown to $\sim$90% confluence in a 6 wells cell culture plate (Greiner, 657160). All hiPSC lines (passage 20-50) were maintained in E8 medium (Gibco, A1517001) for at least three passages before starting cardiac lineage differentiation with media change occurring every day. hiPSC-CM differentiation was performed using small molecule-based Wnt-modulated protocol previously described starting at D0 with RPMI 1640 + L-Glutamine (Life Technologies, 11875-093) supplemented with 2% B-27 supplement minus insulin (Life Technologies, A1895601) and 8 µM CHIR99021 (CHIR) (Selleckchem, S2924), a canonical Wnt pathway activator (via specific GSK3β) inhibition) [11, 26].

At D11, wells that contained more than 80% beating cells were treated with TrypLE Select Enzyme 10X (Gibco, A12177) at 37° C for 10-15 minutes (0,75 mL/well in a 6-well plate). In a 6 wells low attachment plate (Corning Costar, 3471) culture format, spheroid generation was optimized to obtain $\sim$400 µm diameter structures, resulting in seeding 1.2 million cells per mL of RPMI 1640 + L-Glutamine (Life Technologies, 11875-093) supplemented with 2% B27 supplement plus insulin (Life Technologies, 17504-044) with rho-associated coiled-coil protein kinase (ROCK) (1:1000, Roche, S1049). In 96 wells round-bottom ultra-low attachment plate (Corning Costar, 7007) culture format, the number of cells to seed were 7500 and 5000 for 250 µL of RPMI-B27+ins + ROCK (1:1000), allowing for the generation of 1 spheroid per well. The plates were kept on the rotation plate (70 rpm, 37° C, 5% CO_2) until fixation on the final time point. On D12, the spheroids were formed using both formats and spontaneous beating was detected from D12-D13, 2 days after spheroid assembly. Medium exchange ($\sim$1 mL for 6 well format and 166 µL in 96 well format) took place every 2-3 days with previously warmed media in water bath (37° C) till the spheroids were ready to be fixated and assays performed. To ensure the fidelity of the disease model and enhance electrophysiological and mechanical characteristics of hiPSC-derived CMs, a maturation medium was used [27]. In both formats, the media was changed from RPMI-B27+ins to maturation medium around D19-21, depending on the morphology of the spheroids. For a minimum of 3 weeks ($\sim$D42) prior to the characterization and functionality assays were performed, spheroids were kept in this maturation medium, which was also exchanged every 2-3 days (166 µL) [27].

The hCO generation protocol was based, adapted and optimized according to previously established protocols for the formation of 3D cardiac microtissues and self-organizing hCOs [11, 28, 12, 13]. Embryoid body (EB) formation occurred 2 days prior to the start of cardiac differentiation (D-2). This way, $\sim$70% confluent hiPSCs were dissociated with 0.5 mM EDTA (Thermo Fisher, 15575020) (0,5 mL in 6 well format, 3 mL in a T75 flask (Greiner, 658170) waiting 3-5 min, checking for dissociating cells under the microscope. After cell counting, hiPSCs were transferred to a round-bottom ultra-low attachment 96 well plate (Corning Costar, 7007) making up 10000, 7500 and 5000 cells per well where the final volume of E8 + ROCK (1:1000) media was 250 µL. The plate was centrifuged after cell seeding at 200xg for 5 min, and kept in the rotation plate (70 rpm, 37° C, 5% CO_2) throughout the whole experiment, namely until assays could be performed on hCOs. On D-1, E8 medium was refreshed. The differentiation process was followed as described for the spheroid generation protocol with alterations on D2, D6 and D7. Differentiation began on D0, after EBs were formed, as 166 µL of media were removed from each well, adding 166 µL of RPMI-B27-ins supplemented with 4 µM/8 µM of CHIR in each well [28]. After activation on D0 occurred using CHIR, Wnt pathway was inhibited on D2 through exposure to 2 µM of Wnt-C59 (Tocris Bioscience, 5148) for 48h in each well. On

D4, media was refreshed and on D6 it was exchanged to RPMI-B27+ins. Spontaneous beating was to be detected around D6-D8, 8 days after EB assembly. On D7, each well was exposed to 2 µM CHIR for 1h, constituting the last pathway activation step. From D7 onwards, media was exchanged every 2 days until RPMI-B27+ins was exchanged to maturation media on D19-21. hCOs were kept in maturation media for a minimum of 3 weeks ($\sim$D42) until fixation prior to assays execution [27]. Bright-field images were obtained with microscope Olympus CKX41 and further analysed for diameter measurements using the open-source Fiji Software, *ImageJ* (https://imagej.net/software/fiji/).

2.2. β-adrenergic stimulation in cardiac spheroids

On the final time point (D42, upon $\sim$3 weeks of maturation), isoproterenol hydrochloride (ISO) (Tocris, 1747/100), was diluted in the maturation media at a final concentration of 100 nM and added at 37° C to the wells (6-wells format). CTRL and PLN spheroids were treated in the same conditions and bright-field videos were captured after 15 minutes of exposure to ISO, to be analysed to quantify beats per second.

2.3. Immunofluorescence analysis

For immunofluorescence (IF) staining, a recently published protocol was used and optimized [29]. The spheroids and organoids were resuspended in 1 mL 4% paraformaldehyde (PFA) solution (Santa Cruz, 30525-89-4) for 45 min for fixation at 4° C. Spheroids and organoids were labelled using nuclei (DAPI/Hoechst 33342, Invitrogen), CM sarcomeric (α-actinin, Merck, A7811) and CF (Pro-COL1A1, Millipore, ABT257) markers. The samples were imaged using Leica SP8 Confocal Microscope at 63x magnification. Confocal images were analysed with the *ImageJ* software where the relative levels of the α-actinin and pro-COL1A1 proteins were measured. For cell quantification in the microtissues, DAPI/Hoechst positive cells were counted and used for normalization against the target cell marker of interest (α-actinin and Pro-COL1A1). A MaxEntropy threshold was used to measure the DAPI/Hoechst+, α-actinin+ and Pro-COL1A1+ areas.

2.4. Calcium assay

To examine electrophysiology in the generated CTRL and PLN constructs, a 3D-calcium handling assay previously developed in our lab was used. The constructs were loaded with the Cal520 dye (Abcam, ab171868). The Cal520 working solution was prepared on the days of the assay diluting the Cal520 aliquot (2.5 mM stock) 1:1000 with 0,02% Pluronic® F-127 (10% stock, required for successful dye loading according to the manufacturer, Sigma Aldrich, P2443) in FluoroBrite DMEM media (Thermo Fisher, A1896701). Thereafter, the spheroids and organoids were diluted 1:1 with the Cal520 working solution, removing maturation media accordingly. The plates already dye-loaded were incubated in 37° C 5% CO_2 for 1h before the calcium assay was performed. During the incubation step, the microscope was warmed to 37° C. Leica Thunder i8 microscope was used to collect the videos of the Ca^{2+} transient of whole spheroids and organoids with a capture rate of 200 frames per second (8-10 seconds videos) and low exposure. Finally, the video files (AVI) were converted to TIFF format pictures using the *ImageJ* software, and uploaded in the CyteSeer® Automated Video Analysis software (Vala Sciences).

2.5. Statistics

Two-group analysis used the Unpaired Student's t test. The p values for significant differences are visualized as: *p $<$ 0.05, ** p $<$ 0.01, *** p $<$ 0.001, **** p $<$ 0.0001. Data are expressed and plotted as the Mean ± SD as indicated in figure legends. The sample size used in each experiment is indicated in the figure legends. Statistical analysis was performed using GraphPad Prism 8.2.0.

3. Results & Discussion

3.1. Generation of cardiac CTRL and PLN spheroids and organoids

In this project, we aimed to construct a 3D model of the human heart able to recapitulate hallmarks of the PLN R14del cardiomyopathy. To achieve this purpose, two methodologies were developed, optimized and examined.

The spheroid generation protocol is a novel system resulting from extensive literature review that allows for the production of a significant amount of cardiac physiologically-relevant models [15, 13, 14]. The protocol for hiPSC differentiation into CMs for CTRL and PLN R14del cell lines was followed as Figure 2 **A** presents with bright-field images taken at the indicated times (Figure 2 **C**). As stated in literature, most successful cardiac expansion is obtained when started between D10 and D14 and spontaneous contraction in hiPSC-derived CMs monolayers is detected on D11 [30]. Consequently, expansion of CMs was started on D11 along with spheroid formation. After cell recovery from replating, CMs began aggregating seeded in 6 wells low attachment and 96 wells ultra-low attachment culture plates. Regarding cell seeding number, 7500 cells presents no significant diameter change over the course of the experiment for both cell lines. In contrast, using 5000 cells showed a statistically significant increase, possibly indicating that cell-cell contact could be inhibiting CM proliferation as stated in previous reports [26]. Thus, 5000 can be considered as a more valuable option to use as cell seeding number given that spheroids from both cell lines were established and showed significant growth overtime with beating activity. Spontaneous beating was detected after 24-48h of plates incubation in the rotation plate (Figure 2 **G**). Functional spheroids were successfully established as a significant amount of spheroids ($\sim$80%) first started beating after aggregation (D12). Before maturation conditions were applied (D19), 99% showed regular beating. This was observed for both cell lines which supports the robustness and reproducibility of the differentiation and spheroid generation techniques used. Furthermore, at the final time point (D42) after maturation, the beat rate was measured for both conditions, validating the functionality of the spheroids generated (Figure 2 **G**).

Secondly, a different technique was used to focus on establishing a system for 3D culturing of hiPSCs as EBs prior to cardiac differentiation. The end goal of using this different protocol was to obtain a more organoid-like functional structure in the sense that self-organization throughout differentiation in 3D would be possible. This system was adapted from established methodologies in order to create self-organizing morphologically complex hCOs from hiPSCs [11, 28, 12], according to the timeline presented in Figure 2 **B**. hiPSCs aggregation 2 days prior to the start of the differentiation process allows for cardiac differentiation to occur in 3D. The organoids were first kept in an incubator during organoid generation and maintenance. Nevertheless, it was noted that hCOs were not increasing in size and showed an abnormal development attributed to poor medium quality (Figure 5B from the work of Baillie-Johnson et al. [31]). Hence, an adjustment was made for optimized hCOs generation and, for all subsequent experiments and batches analysed in this study, the plates were kept in a rotation plate instead. This proved to enhance proper EB aggregation, size increase and appropriate cardiac differentiation. Allowing for a proper flow of the small molecules and media used, this adjustment circumvented the significant diffusion gradient possibly underlying these problems and more homogeneous hCOs exposure to the components and nutrients was possible. In Figure 2 **D**, whole mount bright-field images of developing hCOs over the course of the experiment show that both CTRL and PLN cell lines were expanding during the experiment, being kept in the rotation plate similar to the cardiac spheroids plates. A significant diameter increase was detected for both cell lines using 5000 and 7500 as cell seeding numbers (Figure 2 **F**), endors-

ing the use of the same numbers for 96-well setup in spheroid formation. Albeit, following Lewis-Israeli et al. [11], 10 000 hiPSCs were seeded in each well. This condition generated abnormal EBs with irregular morphology along development, whose structure was associated with a too high number of cells (Figure 5B from the work of Baillie-Johnson et al. [31]). Furthermore, this condition also reported a much less significant diameter increase overtime (Figure 2 **F**). This can be explained by the possible diffusion gradient of small molecules and nutrients associated with 3D structures during the differentiation process and media refreshing being more striking given the higher cell number. Since CHIR concentration is cell-line-dependent [30, 26], CHIR concentrations of the 24h exposure on D0 were tested (4 µM and 8 µM) [11, 28]. Indeed, a significantly higher amount of hCOs were beating on D15 having been exposed to 4 µM of CHIR for 24h on D0 in comparison with the hCOs exposed to 8 µM (Figure 2 **H**). Thereafter, taking these results into account, for all subsequent batches analysed, 5000 and 7500 hiPSCs were seeded in the 96 wells plate and 4 µM of CHIR was used for the start of cardiac differentiation, since the response to both concentrations tested was similar in both CTRL and PLN cell lines (Figure 2 **H**).

3.2. Cardiac spheroids responsive to β-adrenergic stimulation

After setting up the spheroid system, an evaluation of the constructs' response to β-adrenergic stimulation was performed. For this purpose, a cardioactive drug widely used clinically was selected - isoprenaline (isoproterenol hydrochloride) [32, 33]. Isoproterenol is a β-1 and β-2 adrenergic receptor agonist, binding to the β-adrenergic receptors in CMs. When this happens, a G-alpha stimulatory second messenger system is activated, resulting in adenylate cyclase activation. Subsequently, this enzyme converts intracellular ATP to cyclic AMP (cAMP), which activates protein kinase A (PKA). PKA phosphorylates LTCC in CMs and enhances Ca^{2+} release from the SR via RYR2 channels. Ultimately, this significant increase in intracellular Ca^{2+} concentration translates in heart rate acceleration given the positive inotropic and lusitropic effects of ISO [33, 34].

In Figure 1, it can be seen that CTRL and PLN spheroids presented a $\sim$2.1-fold increase of beating frequency upon administration of ISO. A previous report has demonstrated the same behaviour in hiPSC-CMs cardiac organoids [15], while another one using human heart slices showed a $\sim$2.04-fold increase in contractility [35], which is comparable to the measurements obtained in the present assay. Notably, these results are in concordance with human heart measurements upon isoproterenol administration [36].

Overall, the positive inotropic and lusitropic effects of ISO indicate that the β-adrenergic signaling pathways in hiPSC-CMs within the cardiac spheroids are intact, as a physiologically relevant stimulation is detected. Physiological responses to isoproterenol have also been correlated with tissue maturity when using the same maturation media and time exposure to it as used in this project [37, 27]. Thus, appropriate hiPSC-CMs maturity can be inferred. Consequently, this proof-of-concept experiment of drug responsiveness in the 3D models generated validates the potential physiological functionality. Therefore, this indicates the applicability of the method for possible evaluation and comparison of pathological features between the CTRL and PLN spheroids.

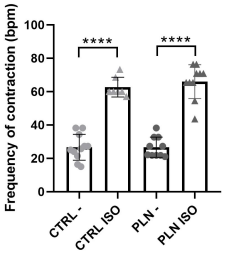

Figure 1: Quantification of the contraction frequency of CTRL and PLN spheroids untreated (-) and treated (ISO) with 100 nM of isoprenaline (3 independent biological replicates, n=10 spheroids per condition, value = mean ± s.d., two-tailed, unpaired t-test, ****$p < 0.0001$).

3.3. Heart spheroids and organoids produce cardiac-specific cell lineages

Firstly, we examined overall morphology and cellular architecture by whole-mount IF staining for nuclei (DAPI/Hoechst), CM (α-actinin) and CF (Pro-COL1A1) markers with fixated structures on D42, after 3 weeks of maturation. These results can be observed in Figure 3.

In Figure 3 **A**, it is noticeable that CMs showing sarcomeric striation were located throughout the entire spheroid, whereas CFs were found interspersed among CMs. Comparing CTRL and PLN spheroids, cellular sorting and architecture in 3D showed no remarkable difference that could be visualized using this assay. The evaluation of the overall spheroid morphology aligned with previous reports also based on the seeding of hiPSC-derived CMs resulting in similar size structures [38, 39]. As for hCOs, in Figure 3 **B**, the self-organization of each cell lineage can be observed and cellular architecture understood using the same CM and CF markers previously specified. Spatial cardiac differentiation was successful and could be observed using CTRL and PLN hiPSCs. Notably, CMs appeared throughout the whole hCO, being more directed towards the perimeter. CFs also seemed to be dispersed in the whole structure, where the PLN R14del also did not seem to be related to any significant cellular organization alteration. These observations are supported by the report from which the methodology was mostly adapted from [11].

Interestingly, we aimed to quantify the contribution of the different cardiac cell populations to the models obtained (Figure 3 **C**, **D**). Evidently, the spheroids were generated from hiPSC-derived CMs whereas the organoids resulted from hiPSCs cardiac differentiation in 3D. This means that disparities in cell ratio were expected between spheroids and organoids as the self-organizing method is associated with a possibly less controlled differentiation process in the EB. Once again, the cellular composition obtained in the spheroids is consistent with other models [13, 40] and the cellular ratio quantified for CTRL hCOs is similar to a previous report, from which the fabrication methodology was adapted [11]. Nonetheless, despite the differences observed, in both systems there is a $\sim$90% and $\sim$73% increase in Pro-COL1A1-positive area from CTRL to PLN spheroids and organoids, respectively.

Taking the previous observations into account, we questioned whether myocardial fibrosis could be recapitulated in the *in vitro* models obtained, given that this is a hallmark of PLN R14del cardiomyopathy. Cardiac fibrosis is characterized by excessive deposition of ECM proteins in the myocardium, disrupting its architecture and ECC with collagen as the main component of the cardiac ECM [41, 10, 42]. The carboxy-terminal propeptide of pro-collagen type 1 is synthesized by CFs and released during the biosynthesis process and deposition of collagen 1, being considered a biomarker of collagen synthesis and cardiac fibrosis [43, 44, 45].

Consequently, the images obtained by whole-mount IF staining of 3D structures were processed to understand the expression of COL1A1 gene in the 3D microenvironment. Pro-COL1A1-positive spheroid area was significantly increased in PLN spheroids at this final time point (Figure 3 **E**). Similarly, Pro-

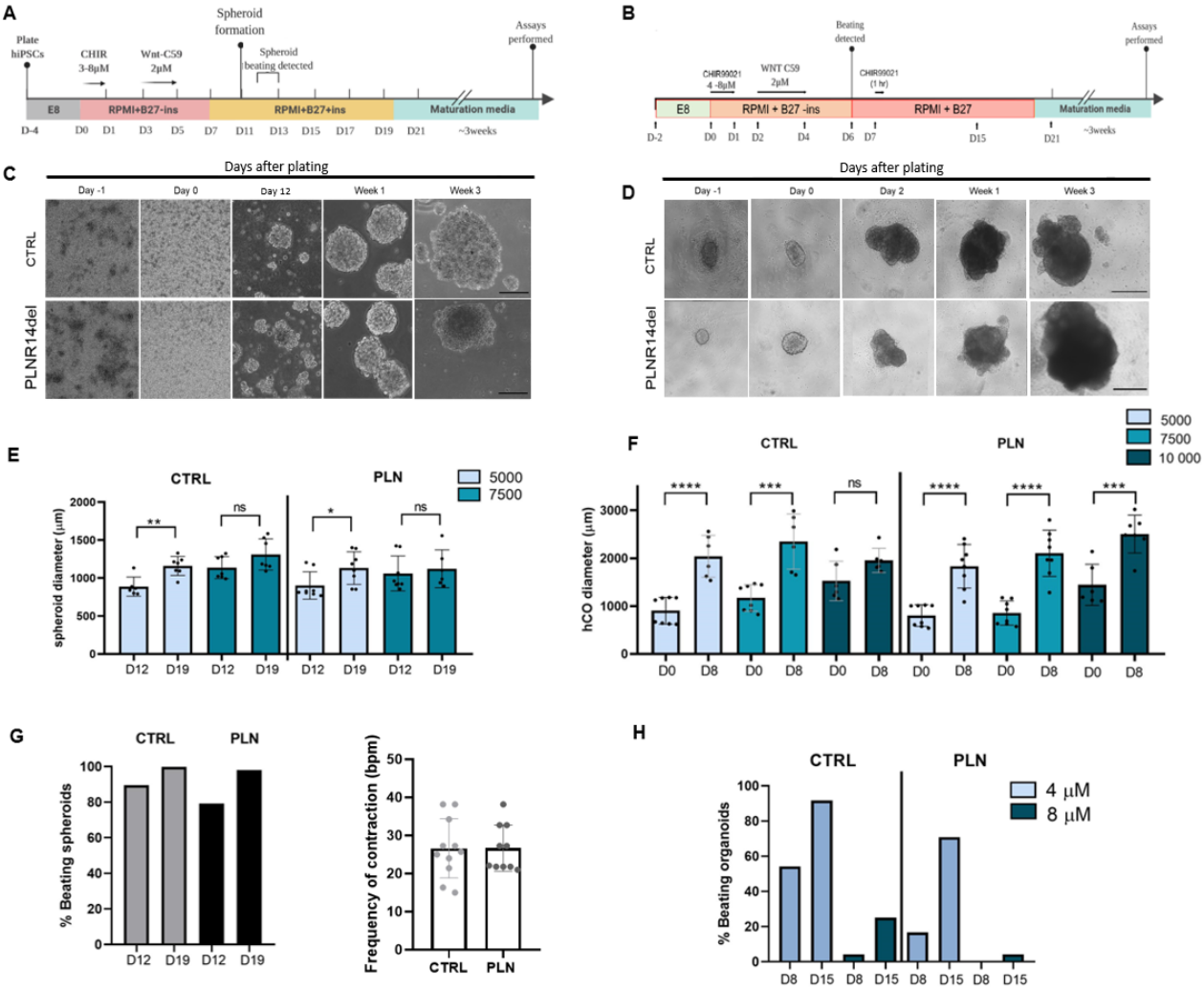

Figure 2: Generation of cardiac spheroids and cardiac organoids from CTRL and PLN R14del hiPSCs. **A**: Cardiac differentiation protocol including spheroid generation steps; **B**: Cardiac differentiation while self-assembling hCOs are generated; **C**: Bright-field images of developing CTRL and PLN spheroids over the course of the experiment (6 wells format). Scale bar: 400 µm; **D**: Brightfield images of developing CTRL and PLN hCOs throughout the differentiation process. Scale bar: 1000 µm; **E**: Quantification of spheroid diameter overtime, according to cell number seeded on a 96 wells format (3 independent biological replicates, n = 8 spheroids per condition, value = mean ± s.d., two-tailed, unpaired t-test, ns: no significance, *$p < 0.05$, **$p < 0.001$); **F**: Quantification of organoid diameter overtime, according to cell number seeded (3 independent biological replicates, n = 8 organoids per condition, value = mean ± s.d., two-tailed, unpaired t-test, ns: no significance, ***$p < 0.001$, ****$p < 0.0001$); **G**: Percentage of beating spheroids from D12 to D19 (3 independent biological replicates). Quantification of the contraction frequency of CTRL and PLN spheroids at D42 (3 independent biological replicates); **H**: Percentage of beating hCOs from D8 to D15 in exposure of different concentrations of CHIR on D0 (2 independent biological replicates).

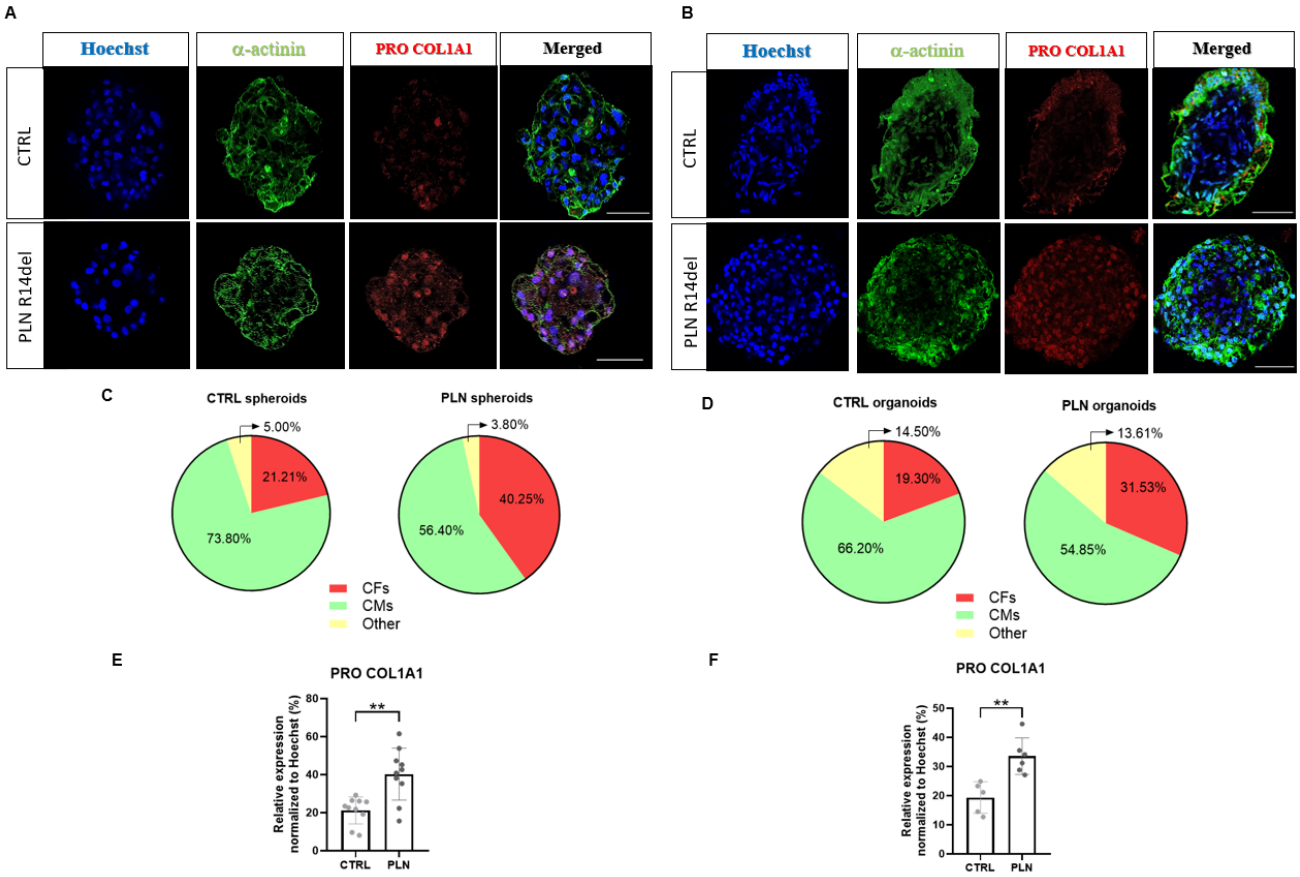

Figure 3: Cellular characterization of CTRL and PLN cardiac spheroids and organoids. **A**: Confocal immunofluorescence images of spheroids at D42 for Hoechst (blue), α-actinin (green), Pro-COL1A1 (red) (CTRL in 96-well format and PLN represents the 6-well format). Scale bar: 50 µm; **B**: Confocal immunofluorescence images of hCOs at D42 according to the same staining conditions as **A**. Scale bar: 50 µm; **C**: Pie charts of average cell composition in cardiac spheroids, calculated as the percentage of cells with respective cell marker over all cells by nuclei counting using ImageJ (4 independent biological replicates, n = 10 spheroids per condition); **D**: Pie charts of average cell composition in hCOs, calculated as the percentage of area with respective cell marker over all cells by nuclei counting using ImageJ (2 independent biological replicates, n = 5 CTRL organoids, n= 7 PLN organoids). **E**: Quantification of Pro-COL1A1+ area in the CTRL and PLN spheroids against total cell area (4 independent biological replicates, n = 10 spheroids per condition, value = mean ± s.d., two-tailed, unpaired t-test, **p=0.001); **F**: Quantification of Pro-COL1A1+ area in the CTRL and PLN hCOs against total cell area (2 independent biological replicates, n = 5 CTRL organoids, n= 7 PLN organoids, value = mean ± s.d., two-tailed, unpaired t-test, **p=0.0032).

COL1A1-positive organoid area showed a significant increase when also normalized to DAPI/Hoechst-positive area (Figure 3 **F**). It is statistically significant that COL1A1's expression was elevated in PLN spheroids and organoids compared with CTRL. This way, a possible recapitulation of myocardial fibrosis may be considered where several pathological features intrinsic to cardiac fibrosis can be underlying this phenotypic behaviour. On account of cardiac fibrosis being a scarring event in the myocardium with pathological alterations, these can comprise an increased collagen type 1 deposition followed by cardiac fibroblast activation and transdifferentiation into myofibroblasts [46, 47].

Once fibroblasts are activated, proliferation and migration capacity are increased and this is accompanied by abundant ECM synthesis and deposition, showing increases in fibrillar collagens in the ECM [43, 46]. Withal, myofibroblasts are phenotypically modulated and characterized by the expression of α-smooth muscle actin (α-SMA) in organized stress fibers. They show enhanced migratory, proliferative and secretory properties, being essential to fibrosis formation [42, 48, 10]. As described, several distinct pathological scenarios can be the reason for a significant enhancement of COL1A1 expression. Besides, an alternative cause for this observation could be unpure differentiation of hiPSC-derived CMs prior to spheroid formation and unpure differentiation process of the hiPSC-EBs.

3.4. Ca^{2+} handling impairment in PLN R14del models

Malignant ventricular arrhythmias are another key pathological feature of PLN R14del cardiomyopathy in human patients. To further investigate this, Ca^{2+} handling properties were measured, namely, Ca^{2+} handling of CMs in the spheroids and hCOs during ECC, including Ca^{2+} transient pattern and kinetics using fluorescent Ca^{2+} imaging. In Figure 4 **B** and **E**, the corresponding Ca^{2+} transients of the constructs can be seen. These results indicate that the spheroids and hCOs generated presented cardiac-like Ca^{2+} transients, which in turn translated into contractions.

Regarding the Ca^{2+} sparks represented in Figure 4 **A** and **D**, it is possible to note that for both PLN models, the Ca^{2+} dye intensity is slightly lower which can be related to the decreased SR Ca^{2+} storage. PLN R14del has a super inhibitory effect on SERCA2a, causing a blockage in Ca^{2+} reuptake in the SR. This means that the SR Ca^{2+} content decreases and, consequently, less Ca^{2+} in the SR is available for subsequent contractions. Additionally, in Figure 4 **B** and **E**, the CTRL showed regular Ca^{2+} sparks, whereas PLN R14del constructs showed a-synchronized Ca^{2+} sparks, potentially indicating an arrhythmic Ca^{2+} cycling profile [7].

CTD25 and CTD75 together account for the overall duration of the Ca^{2+} transient which is shortened in PLN. This is supported by the decreased Decay Time for both models, where Decay Time represents the time SERCA2a takes to reuptake Ca^{2+} back in the SR. Several factors could be underlying this response. More specifically, this could also be an indicator on the depressed SR Ca^{2+} content, that will contribute to a lower amount of Ca^{2+} being present in the cytosol for contraction. Hence, during relaxation, given low Ca^{2+} cytosolic concentration, impaired SERCA2a will pump it into the SR at a higher rate than CTRL, where a greater concentration of Ca^{2+} needs to be reuptaken for relaxation to occur [49]. Essentially, this assay can indicate there is indeed abnormal Ca^{2+} handling connected with the PLN R14del mutation. However, the observation of Ca^{2+} transient pattern and kinetics is not enough to properly understand the high frequency of ventricular arrhythmias in PLN R14del cardiomyopathy.

4. Experimental Limitations and Future Work

In an attempt to elucidate the still elusive PLN R14del pathophysiology, the assays established were amenable and robust to be performed in a middle-high throughput manner. Even though the experiments allowed for a clear visualization and detection of pathological phenotype features (such as cardiac fibrotic remodelling and Ca^{2+} mishandling), their clear cause, possible direct link or connection to disease severity was not possible to unravel. Adjustments should be considered to improve on the findings of this study.

Overall, across all assays, more replicates of hCOs batches are necessary. On the spheroid generation methodology, it would be valuable to co-culture hiPSC-derived CFs and endothelial cells (ECs) alongside the CMs. This way, more cardiac cell types would be present and a better representation of the human heart could be obtained.

As for the immunostaining assay, it can be an appropriate method for visualization purposes but not entirely for precise quantification. For a complete understanding of cellular architecture and composition, staining of more cardiac specific cell types is also crucial (ECs, endocardial and epicardial cells).As discussed before, staining for α-smooth muscle actin (marker for myofibroblasts) could help towards shedding light on the exact fibrosis scenario associated with PLN R14del cardiomyopathy. After considering all the enumerated constraints, the assay performed here also needs further validation for a robust and reliable cellular characterization and evaluation of cardiac fibrosis as it is highly user-dependent and low throughput. Fluorescence-activated cell sorting (FACS) could be an extra assay performed, allowing for a differentiation efficiency quality control step prior to spheroid formation and, on the final time point, for both 3D systems, to better understand cellular content in the models generated.

Taking into consideration both the complexity of the cardiac arrhythmic scenario in general, and the still unclear cause of the arrhythmic behaviour in PLN R14del cardiomyopathy, different assays should taken into consideration. Possibly, applying the previously established Ca^{2+} quantification assay [50] could help bridging knowledge gaps, measuring Ca^{2+} content of the SR, whether confirming or rejecting the hypothesis presented based on Ca^{2+} content.

5. Conclusions

The present study sought to respond to the pressing need for an adult human heart model, having established promising methodologies. The spheroid and organoid systems were successfully developed and adapted, being able to confirm the pathological features related to PLN R14del cardiomyopathy.

Regarding myocardial fibrosis, a fibrotic behaviour was indeed detected in a 3D microenvironment, which is highly relevant in a human disease scenario with various components possibly underlying the readout. Ca^{2+} mishandling was also identified given the irregular Ca^{2+} transient pattern observed in the PLN R14del models, attributed to a wide variety of distinct arrhythmic elements. Unraveling such specific pathological mechanisms should be the focus of research in the future in order to find ways to delay or revert the disease's natural course and severity progression.

Importantly, the poor prognosis associated with PLN R14del cardiomyopathy and the absence of an available therapy is a strong concern. Therefore, both methodologies developed showed potential to be implemented for drug screenings in a patient-specific high-throughput manner using their hiPSCs. Being adjustable to a 96-well format, both platforms enable the culture of one construct per well, where the tracking of individual hCOs under specific conditions is possible. This opens new avenues for target identification and efficient therapeutic intervention, potentiating new personalized medicine approaches.

6. Acknowledgements

hiPSC and CMs generation until D11 were kindly performed by Renee Maas along the duration of the project. We also thank the Stanford CVI iPSC Biobank and Prof. Mark Mercola for pro-

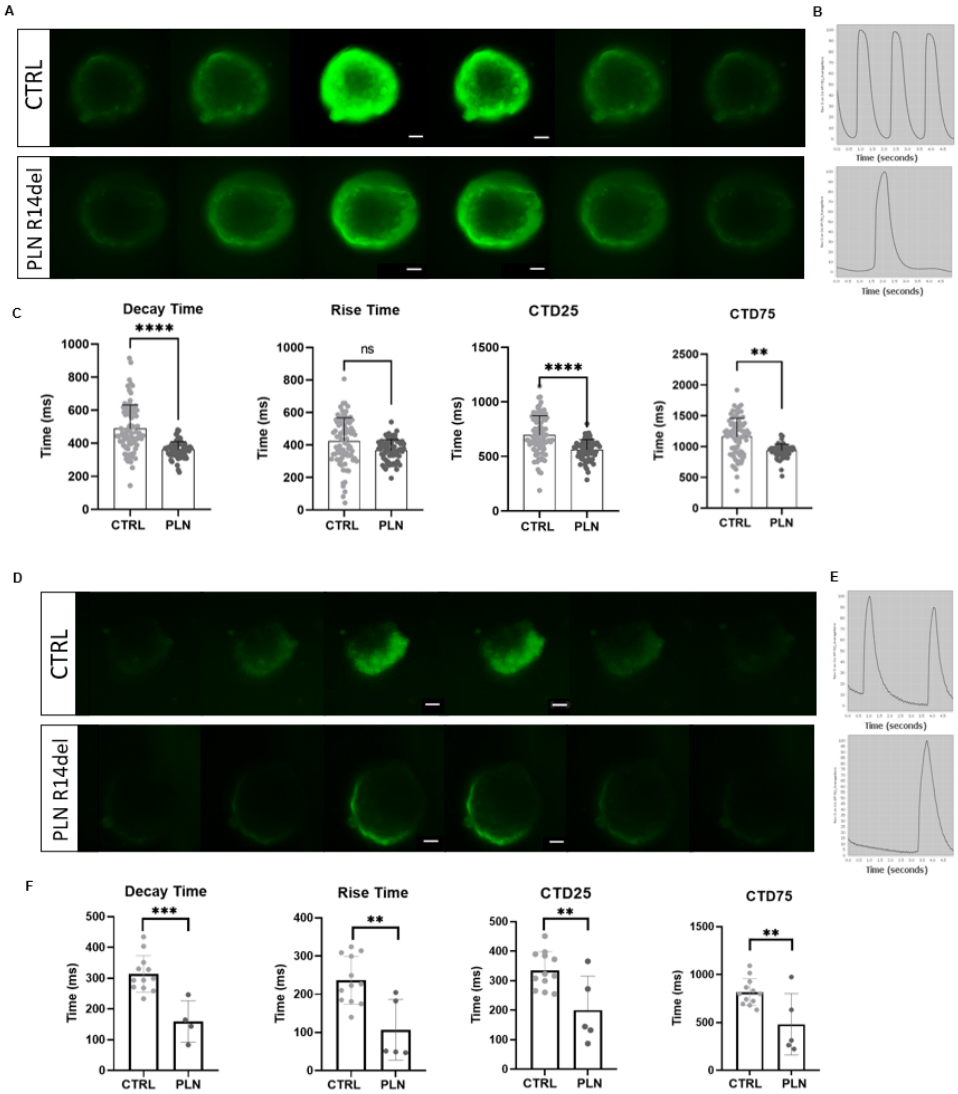

Figure 4: Functional characteristics of CTRL and PLN R14del spheroids and organoids. **A**: Ca^{2+} imaging over time in cardiac spheroids, displaying one Ca^{2+} spark for both conditions (96-well format for CTRL and 6-well format for PLN). Scale bar: 20 µm; **B**: The apparent Ca^{2+} intensity of the respective CTRL and PLN spheroids presented in **A**, recorded in 7 sec, with a total of 255 frames; **C**: Quantification of Ca^{2+} transient parameters in CTRL and PLN spheroids: decay time, rise time, CTD25 and CTD75 (6 independent biological replicates, n = 62 CTRL spheroids, n = 40 PLN spheroids, value = mean ± s.d., two-tailed, unpaired t-test, ns: no significance, **p=0.002, ****p$<$ 0.0001); **D**: Ca^{2+} imaging over time in hCOs, displaying one Ca^{2+} spark for both conditions. Scale bar: 20 µm; **E**: The apparent Ca^{2+} intensity of the respective CTRL and PLN hCOs presented in **D**, recorded in 7 sec, with a total of 255 frames; **F**: Quantification of Ca^{2+} transient parameters in CTRL and PLN organoids: decay time, rise time, CTD25 and CTD75 (2 independent biological replicates, n = 12 CTRL hCOs, n = 5 PLN hCOs, value = mean ± s.d., two-tailed, unpaired t-test, **p=0.0026 (Rise time), **p=0.0065 (CTD25), **p= 0.0074 (CTD75), ***p=0.0006

viding the control and patient iPSC lines. We are very thankful to Vala sciences for providing the valuable software package for the Ca^{2+} handling analysis. I gratefully acknowledge the help of Christian Snijders-Blok, Inge Dokter, Dr. Jan Willem Buikema and Prof. Dr. Joost Sluijter.

References

[1] "Cardiovascular diseases (cvds)." `https://www.who.int/en/news-room/fact-sheets/detail/cardiovascular-diseases-(cvds)`. Accessed on: 10-04-2021.

[2] G. Gilbert, K. Demydenko, E. Dries, R. D. Puertas, X. Jin, K. Sipido, and H. L. Roderick, "Calcium signaling in cardiomyocyte function," *Cold Spring Harbor perspectives in biology*, vol. 12, no. 3, p. a035428, 2020.

[3] M. M. DeWitt, H. M. MacLeod, B. Soliven, and E. M. McNally, "Phospholamban r14 deletion results in late-onset, mild, hereditary dilated cardiomyopathy," *Journal of the American College of Cardiology*, vol. 48, no. 7, pp. 1396–1398, 2006.

[4] H. Sutanto, A. Lyon, J. Lumens, U. Schotten, D. Dobrev, and J. Heijman, "Cardiomyocyte calcium handling in health and disease: insights from in vitro and in silico studies," *Progress in biophysics and molecular biology*, vol. 157, pp. 54–75, 2020.

[5] N. Bögeholz, A. Muszynski, and C. Pott, "The physiology of cardiac calcium handling," *Wiener medizinische Wochenschrift*, vol. 162, no. 13, pp. 278–282, 2012.

[6] T. R. Eijgenraam, B. J. Boukens, C. J. Boogerd, E. M. Schouten, C. W. van de Kolk, N. M. Stege, W. P. Te Rijdt, E. T. Hoorntje, P. A. van der Zwaag, E. van Rooij, *et al.*, "The phospholamban p.(arg14del) pathogenic variant leads to cardiomyopathy with heart failure and is unresponsive to standard heart failure therapy," *Scientific reports*, vol. 10, no. 1, pp. 1–13, 2020.

[7] I. Karakikes, F. Stillitano, M. Nonnenmacher, C. Tzimas, D. Sanoudou, V. Termglinchan, C.-W. Kong, S. Rushing, J. Hansen, D. Ceholski, *et al.*, "Correction of human phospholamban r14del mutation associated with cardiomyopathy using targeted nucleases and combination therapy," *Nature communications*, vol. 6, no. 1, pp. 1–10, 2015.

[8] I. Hof, J. Van der Heijden, E. Kranias, D. Sanoudou, R. De Boer, J. Van Tintelen, P. van der Zwaag, and P. Doevendans, "Prevalence and cardiac phenotype of patients with a phospholamban mutation," *Netherlands Heart Journal*, vol. 27, no. 2, pp. 64–69, 2019.

[9] A. G. Japp, A. Gulati, S. A. Cook, M. R. Cowie, and S. K. Prasad, "The diagnosis and evaluation of dilated cardiomyopathy," *Journal of the American College of Cardiology*, vol. 67, no. 25, pp. 2996–3010, 2016.

[10] T. R. Eijgenraam, H. H. Silljé, and R. A. de Boer, "Current understanding of fibrosis in genetic cardiomyopathies," *Trends in cardiovascular medicine*, vol. 30, no. 6, pp. 353–361, 2020.

[11] Y. R. Lewis-Israeli, A. H. Wasserman, M. A. Gabalski, B. D. Volmert, Y. Ming, K. A. Ball, W. Yang, J. Zou, G. Ni, N. Pajares, *et al.*, "Self-assembling human heart organoids for the modeling of cardiac development and congenital heart disease," *Nature Communications*, vol. 12, no. 1, pp. 1–16, 2021.

[12] L. Drakhlis, S. Biswanath, C.-M. Farr, V. Lupanow, J. Teske, K. Ritzenhoff, A. Franke, F. Manstein, E. Bolesani, H. Kempf, *et al.*, "Human heart-forming organoids recapitulate early heart and foregut development," *Nature Biotechnology*, pp. 1–10, 2021.

[13] E. Giacomelli, V. Meraviglia, G. Campostrini, A. Cochrane, X. Cao, R. W. Van Helden, A. K. Garcia, M. Mircea, S. Kostidis, R. P. Davis, *et al.*, "Human-ipsc-derived cardiac stromal cells enhance maturation in 3d cardiac microtissues and reveal non-cardiomyocyte contributions to heart disease," *Cell stem cell*, vol. 26, no. 6, pp. 862–879, 2020.

[14] P. Andersen, E. Tampakakis, D. V. Jimenez, S. Kannan, M. Miyamoto, H. K. Shin, A. Saberi, S. Murphy, E. Sulistio, S. P. Chelko, *et al.*, "Precardiac organoids form two heart fields via bmp/wnt signaling," *Nature communications*, vol. 9, no. 1, pp. 1–13, 2018.

[15] D. J. Richards, R. C. Coyle, Y. Tan, J. Jia, K. Wong, K. Toomer, D. R. Menick, and Y. Mei, "Inspiration from heart development: Biomimetic development of functional human cardiac organoids," *Biomaterials*, vol. 142, pp. 112–123, 2017.

[16] A. Mathur, P. Loskill, K. Shao, N. Huebsch, S. Hong, S. G. Marcus, N. Marks, M. Mandegar, B. R. Conklin, L. P. Lee, *et al.*, "Human ipsc-based cardiac microphysiological system for drug screening applications," *Scientific reports*, vol. 5, p. 8883, 2015.

[17] X. Lian, X. Bao, M. Zilberter, M. Westman, A. Fisahn, C. Hsiao, L. B. Hazeltine, K. K. Dunn, T. J. Kamp, and S. P. Palecek, "Chemically defined, albumin-free human cardiomyocyte generation," *Nature methods*, vol. 12, no. 7, pp. 595–596, 2015.

[18] P. W. Burridge, E. Matsa, P. Shukla, Z. C. Lin, J. M. Churko, A. D. Ebert, F. Lan, S. Diecke, B. Huber, N. M. Mordwinkin, *et al.*, "Chemically defined generation of human cardiomyocytes," *Nature methods*, vol. 11, no. 8, pp. 855–860, 2014.

[19] G. V. Novakovic, T. Eschenhagen, and C. Mummery, "Myocardial tissue engineering: in vitro models," *Cold Spring Harbor perspectives in medicine*, vol. 4, no. 3, p. a014076, 2014.

[20] M. A. Lancaster and J. A. Knoblich, "Organogenesis in a dish: modeling development and disease using organoid technologies," *Science*, vol. 345, no. 6194, p. 1247125, 2014.

[21] Y.-R. Lou and A. W. Leung, "Next generation organoids for biomedical research and applications," *Biotechnology advances*, vol. 36, no. 1, pp. 132–149, 2018.

[22] A. Saini, "Cystic fibrosis patients benefit from mini guts," *Cell Stem Cell*, vol. 19, no. 4, pp. 425–427, 2016.

[23] P. Politi, M. Piccinelli, P. F. Poli, C. Klersy, C. Campana, C. Goggi, M. Viganò, and F. Barale, "Ten years of "extended" life: quality of life among heart transplantation survivors," *Transplantation*, vol. 78, no. 2, pp. 257–263, 2004.

[24] E. Matsa, P. W. Burridge, K.-H. Yu, J. H. Ahrens, V. Termglinchan, H. Wu, C. Liu, P. Shukla, N. Sayed, J. M. Churko, *et al.*, "Transcriptome profiling of patient-specific human ipsc-cardiomyocytes predicts individual drug safety and efficacy responses in vitro," *Cell stem cell*, vol. 19, no. 3, pp. 311–325, 2016.

[25] D. A. Feyen, I. Perea-Gil, R. G. Maas, M. Harakalova, A. A. Gavidia, J. Arthur Ataam, T.-H. Wu, A. Vink, J. Pei, N. Vadgama, *et al.*, "The unfolded protein response as a compensatory mechanism and potential therapeutic target in pln r14del cardiomyopathy," *Circulation*, 2021.

[26] J. W. Buikema, S. Lee, W. R. Goodyer, R. G. Maas, O. Chirikian, G. Li, Y. Miao, S. L. Paige, D. Lee, H. Wu, *et al.*, "Wnt activation and reduced cell-cell contact synergistically induce massive expansion of functional human ipsc-derived cardiomyocytes," *Cell stem cell*, vol. 27, no. 1, pp. 50–63, 2020.

[27] D. A. Feyen, W. L. McKeithan, A. A. Bruyneel, S. Spiering, L. Hörmann, B. Ulmer, H. Zhang, F. Briganti, M. Schweizer, B. Hegyi, *et al.*, "Metabolic maturation media improve physiological function of human ipsc-derived cardiomyocytes," *Cell reports*, vol. 32, no. 3, p. 107925, 2020.

[28] P. Hofbauer, S. M. Jahnel, N. Papai, M. Giesshammer, A. Deyett, C. Schmidt, M. Penc, K. Tavernini, N. Grdseloff, C. Meledeth, *et al.*, "Cardioids reveal self-organizing principles of human cardiogenesis," *Cell*, 2021.

[29] R. L. van Ineveld, H. C. Ariese, E. J. Wehrens, J. F. Dekkers, and A. C. Rios, "Single-cell resolution three-dimensional imaging of intact organoids," *JoVE (Journal of Visualized Experiments)*, no. 160, p. e60709, 2020.

[30] R. G. Maas, S. Lee, M. Harakalova, C. J. S. Blok, W. R. Goodyer, J. Hjortnaes, P. A. Doevendans, L. W. Van Laake, J. van der Velden, F. W. Asselbergs, *et al.*, "Massive expansion and cryopreservation of functional human induced pluripotent stem cell-derived cardiomyocytes," *STAR protocols*, vol. 2, no. 1, p. 100334, 2021.

[31] P. Baillie-Johnson, S. C. Van den Brink, T. Balayo, D. A. Turner, and A. M. Arias, "Generation of aggregates of mouse embryonic stem cells that show symmetry breaking, polarization and emergent collective behaviour in vitro," *Journal of visualized experiments: JoVE*, no. 105, 2015.

[32] T. C. Stummann, M. Wronski, T. Sobanski, B. Kumpfmueller, L. Hareng, S. Bremer, and M. P. Whelan, "Digital movie analysis for quantification of beating frequencies, chronotropic effects, and beating areas in cardiomyocyte cultures," *Assay and drug development technologies*, vol. 6, no. 3, pp. 375–385, 2008.

[33] M. W. Szymanski and D. P. Singh, "Isoproterenol," 2018.

[34] S. Alhayek and C. V. Preuss, "Beta 1 receptors," *StatPearls [Internet]*, 2020.

[35] M. Brandenburger, J. Wenzel, R. Bogdan, D. Richardt, F. Nguemo, M. Reppel, J. Hescheler, H. Terlau, and A. Dendorfer, "Organotypic slice culture from human adult ventricular myocardium," *Cardiovascular research*, vol. 93, no. 1, pp. 50–59, 2012.

[36] J. R. Stratton, M. D. Cerqueira, R. S. Schwartz, W. C. Levy, R. Veith, S. E. Kahn, and I. B. Abrass, "Differences in cardiovascular responses to isoproterenol in relation to age and exercise training in healthy men.," *Circulation*, vol. 86, no. 2, pp. 504–512, 1992.

[37] K. Ronaldson-Bouchard, S. P. Ma, K. Yeager, T. Chen, L. Song, D. Sirabella, K. Morikawa, D. Teles, M. Yazawa, and G. Vunjak-Novakovic, "Advanced maturation of human cardiac tissue grown from pluripotent stem cells," *Nature*, vol. 556, no. 7700, pp. 239–243, 2018.

[38] P. Beauchamp, C. B. Jackson, L. C. Ozhathil, I. Agarkova, C. L. Galindo, D. B. Sawyer, T. M. Suter, and C. Zuppinger, "3d co-culture of hipsc-derived cardiomyocytes with cardiac fibroblasts improves tissue-like features of cardiac spheroids," *Frontiers in molecular biosciences*, vol. 7, p. 14, 2020.

[39] L. Polonchuk, M. Chabria, L. Badi, J.-C. Hoflack, G. Figtree, M. J. Davies, and C. Gentile, "Cardiac spheroids as promising in vitro models to study the human heart microenvironment," *Scientific reports*, vol. 7, no. 1, pp. 1–12, 2017.

[40] H. K. Voges, R. J. Mills, D. A. Elliott, R. G. Parton, E. R. Porrello, and J. E. Hudson, "Development of a human cardiac organoid injury model reveals innate regenerative potential," *Development*, vol. 144, no. 6, pp. 1118–1127, 2017.

[41] C. Yang, S. Qiao, Y. Song, Y. Liu, Y. Tang, L. Deng, J. Yuan, F. Hu, and W. Yang, "Procollagen type i carboxy-terminal propeptide (picp) and mmp-2 are potential biomarkers of myocardial fibrosis in patients with hypertrophic cardiomyopathy," *Cardiovascular Pathology*, vol. 43, p. 107150, 2019.

[42] L. Li, Q. Zhao, and W. Kong, "Extracellular matrix remodeling and cardiac fibrosis," *Matrix biology*, vol. 68, pp. 490–506, 2018.

[43] L. S. Neff and A. D. Bradshaw, "Cross your heart? collagen cross-links in cardiac health and disease," *Cellular Signalling*, vol. 79, p. 109889, 2021.

[44] A. G. Raafs, J. A. Verdonschot, M. T. Henkens, B. P. Adriaans, P. Wang, K. Derks, M. A. A. Hamid, C. Knackstedt, V. P. van Empel, J. Díez, *et al.*, "The combination of carboxy-terminal propeptide of procollagen type i blood levels and late gadolinium enhancement at cardiac magnetic resonance provides additional prognostic information in idiopathic dilated cardiomyopathy–a multilevel assessment of myocardial fibrosis in dilated cardiomyopathy," *European Journal of Heart Failure*, vol. 23, no. 6, p. 933, 2021.

[45] B. López, A. González, N. Varo, C. Laviades, R. Querejeta, and J. Díez, "Biochemical assessment of myocardial fibrosis in hypertensive heart disease," *Hypertension*, vol. 38, no. 5, pp. 1222–1226, 2001.

[46] S. Hinderer and K. Schenke-Layland, "Cardiac fibrosis–a short review of causes and therapeutic strategies," *Advanced drug delivery reviews*, vol. 146, pp. 77–82, 2019.

[47] M.-O. Lee, K. B. Jung, S.-J. Jo, S.-A. Hyun, K.-S. Moon, J.-W. Seo, S.-H. Kim, and M.-Y. Son, "Modelling cardiac fibrosis using three-dimensional cardiac microtissues derived from human embryonic stem cells," *Journal of biological engineering*, vol. 13, no. 1, pp. 1–17, 2019.

[48] T. C. Bracco Gartner, J. C. Deddens, E. A. Mol, M. Magin Ferrer, L. W. Van Laake, C. V. Bouten, A. Khademhosseini, P. A. Doevendans, W. J. Suyker, J. P. Sluijter, *et al.*, "Anti-fibrotic effects of cardiac progenitor cells in a 3d-model of human cardiac fibrosis," *Frontiers in cardiovascular medicine*, vol. 6, p. 52, 2019.

[49] N. Sun, M. Yazawa, J. Liu, L. Han, V. Sanchez-Freire, O. J. Abilez, E. G. Navarrete, S. Hu, L. Wang, A. Lee, *et al.*, "Patient-specific induced pluripotent stem cells as a model for familial dilated cardiomyopathy," *Science translational medicine*, vol. 4, no. 130, pp. 130ra47–130ra47, 2012.

[50] H. S. Hwang, D. O. Kryshtal, T. K. Feaster, V. Sánchez-Freire, J. Zhang, T. J. Kamp, C. C. Hong, J. C. Wu, and B. C. Knollmann, "Comparable calcium handling of human ipsc-derived cardiomyocytes generated by multiple laboratories," *Journal of molecular and cellular cardiology*, vol. 85, pp. 79–88, 2015.